Frequency Reconfigurable Pixelated Antenna Using VO_2 Phase Transition Material

Zhanlong Lou
School of Microelectronics
Hefei University of Technology
Hefei, China
2022214881@mail.hfut.edu.cn

Lele Liao
School of Microelectronics
Hefei University of Technology
Hefei, China
2024214944@mail.hfut.edu.cn

Yujie Wang
School of Microelectronics
Hefei University of Technology
Hefei, China
2871542234@qq.com

Yu Yang
School of Microelectronics
Hefei University of Technology
Hefei, China
yy3523516425@outlook.com

Junlin Li
School of Microelectronics
Hefei University of Technology
Hefei, China
1355661653@qq.com

Shuyao Yan*
School of Microelectronics
Hefei University of Technology
Hefei, China
yanshuyaouestc@163.com

2025 IEEE 8th International Symposium on Electromagnetic Compatibility (ISEMC) | 979-8-3315-7915-9/25/$31.00 ©2025 IEEE | DOI: 10.1109/ISEMC68048.2025.11292577

***Abstract*—This paper presents a frequency-reconfigurable pixelated antenna utilizing vanadium dioxide (VO_2) phase-transition control. Three distinct operating modes spanning C-X band are established through thermal reconfiguration of dynamically mapped radiating surfaces: a low-frequency mode (5.48-5.62 GHz) forming a bisymmetric patch, a mid-frequency mode (6.52-6.56 GHz) implementing a W-shaped structure, and a high frequency mode (8.77-8.99 GHz) generating a triangular topology. The antenna features a simple, fabrication-friendly layout whose radiation performance depends critically on VO_2 film quality-specifically, the conductivity contrast between insulating and metallic phases. Higher conductivity differentials yield superior radiation characteristics, achieving gains of 6.25-8.45 dBi with stabilized beam pointing at -43° to -39° . Unlike RF-MEMS and other electronically tuned alternatives, this design eliminates bias circuitry, significantly reducing implementation complexity and positioning it as a high potential solution for adaptive wireless communication systems.**

Keywords—Frequency Reconfigurable; Pixel Antenna; Vanadium Dioxide; Microstrip Patch Antenna

I. INTRODUCTION

In recent years, rapid upgrades in wireless communication systems have triggered antenna proliferation and significantly increased structural complexity within shared platforms [1]. Traditional fixed-frequency antennas, limited to single-band operation, struggle to dynamically adapt to multi-band communication demands amid spectrum scarcity [2]. Frequency reconfigurable technology effectively addresses this challenge by dynamically adjusting antenna structures or electrical parameters to achieve multi-band switching, thereby substantially improving spectrum utilization efficiency [3].

Current reconfigurable microwave devices predominantly utilize RF-MEMS switches, PIN diodes, and varactor diodes for tuning [4][5]. These approaches, however, are limited to stepwise reconfiguration and suffer from compromised stability and durability. Research confirms that VO_2 undergoes a reversible phase transition from monocleinic to tetragonal rutile structure at $\approx 68^\circ$ C, accompanied by an abrupt conductivity jump of 4-6 orders of magnitude [6]. This exceptional property enables VO_2 to replace conventional electronic tuning components.

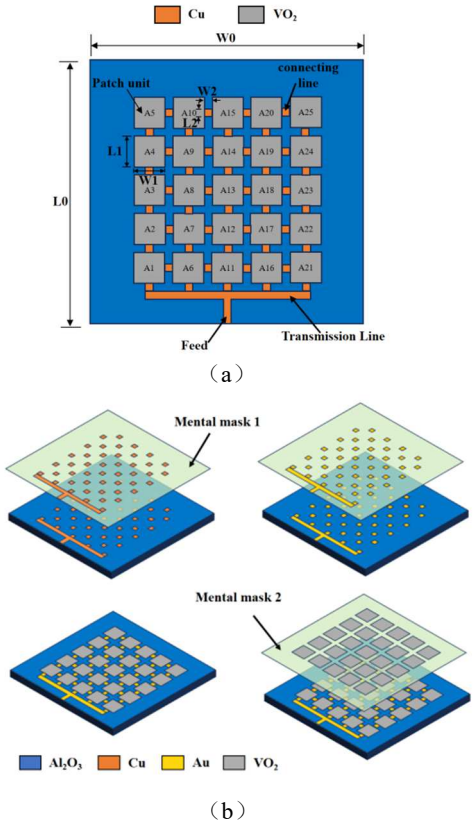

Fig. 1. (a) Schematic diagram of reconfigurable pixel array antenna structure; (b) Top view of antenna manufacturing process.

TABLE I. ANTENNA STRUCTURE PARAMETERS

UNIT: MM

W_0	L_0	W_1	L_1	W_2	L_2
44.00	42.50	5.00	5.00	1.25	1.25

This paper presents the design of a frequency-reconfigurable pixel array antenna leveraging the phase-change characteristics of VO_2 thin films. A novel pixelated architecture is constructed by discretizing a conventional microstrip patch antenna and interconnecting the resulting array elements. Innovatively, VO_2 thin films are employed to form the array elements themselves, functioning as thermally controlled switches rather than relying on conventional

electronic tuning components. By selectively switching the conductivity of specific units via thermal actuation, dynamically reconfigurable radiating surfaces of varying geometries can be realized. This approach effectively emulates the electromagnetic behavior of a microstrip patch antenna with dynamically variable size and shape. Consequently, radiation control analogous to pixel-based imaging is achieved. The implemented design successfully demonstrates a reconfigurable antenna capable of operating across three independent frequency bands spanning the C to X band.

II. Reconfigurable Antenna Design

A. Antenna Manufacturing

Fig. 1(a) illustrates a microstrip line-fed 5×5 uniformly sized pixelated antenna array. The structure was fabricated on a 2 mm thick Rogers RT/duroid 5880 substrate using a CMOS-compatible process flow. As depicted in Fig. 1(b), the T-junction feed structure and array interconnects were metallized with a 1 μm thick copper layer deposited via electron-beam evaporation. To prevent copper oxidation, a 20 nm thick gold capping layer was subsequently evaporated. Twenty-five 1 μm thick VO_2 films were then patterned on the substrate surface by DC magnetron sputtering [7], defining the array elements labeled A1-A25.

B. Antenna surface size design

Given the thermally activated phase-transition mechanism in this design, the layout optimization must account for heat transfer effects to implement a critical unit cell spacing of L_2 = 1.25 mm, satisfying thermal crosstalk constraints as governed by:

$$\Delta d > 2\sqrt{\alpha\tau}\ln\left(\frac{T_c - T_0}{T_{th} - T_0}\right) \quad (1)$$

With critical thermal parameters defined as phase transition point T_c=68°C, spurious activation threshold T_{th}=45°C, and substrate thermal diffusivity α=5.2×10^{-6} m^2/s, localized phase transition is ensured exclusively within target elements.

For all operating modes (Antenna 1-3), TM_{02} mode excitation is observed. As evidenced in Figs. 2(b), 3(b), and 4(b), surface currents exhibit two antinodes along the resonant direction (x-axis) with a central node, maintaining radiation pattern similarity across configurations. The operational frequency follows:

$$f_{TM_{02}} = \frac{c}{2(L + \Delta L)\sqrt{\varepsilon_{eff}}} \quad (2)$$

Where ε_{eff} denotes the effective dielectric constant and ΔL represents the fringing field extension length. Progressive reduction of the resonant array length L from antenna 1 to antenna 3 increases operational frequency while preserving directional characteristics, enabling frequency reconfigurability. Critical dimensions are summarized in Table I.

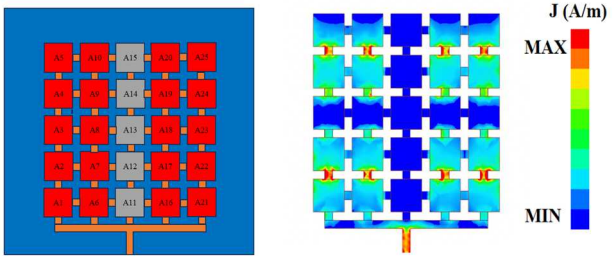

Fig. 2. (a) Radiation pattern on the surface of antenna 1; (b) Current distribution on the surface of antenna 1.

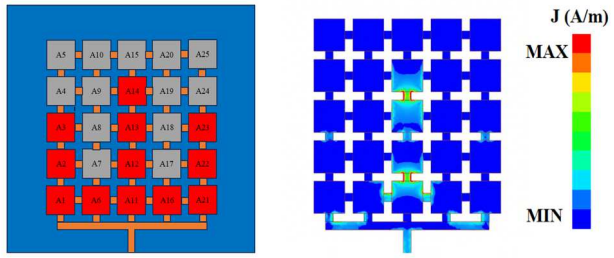

Fig. 3. (a) Radiation pattern on the surface of antenna 2; (b) Current distribution on the surface of antenna 2.

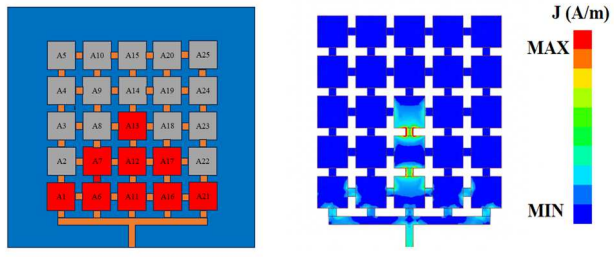

Fig. 4. a) Radiation pattern on the surface of antenna 3; (b) Current distribution on the surface of antenna 3.

III. Simulation Results

When array elements A1-A25 are thermally activated to the conductive state (Antenna 1, Fig. 2(a)), the pixelated structure forms two electromagnetically coupled symmetric patches. This configuration exhibits increased electrical length, resulting in a fundamental resonance at 5.56 GHz (Fig. 5). The radiation pattern in Fig. 6(a) demonstrates a maximum gain of 7.15 dB at elevation angle θ = -42° in the *xOz* plane, with a main lobe beamwidth of 52.99° spanning -72.39° to 19.4°.

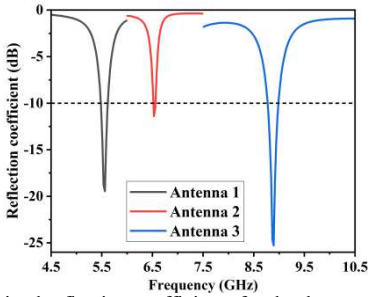

Fig. 5. The obtained reflection coefficients for the three antenna patterns.

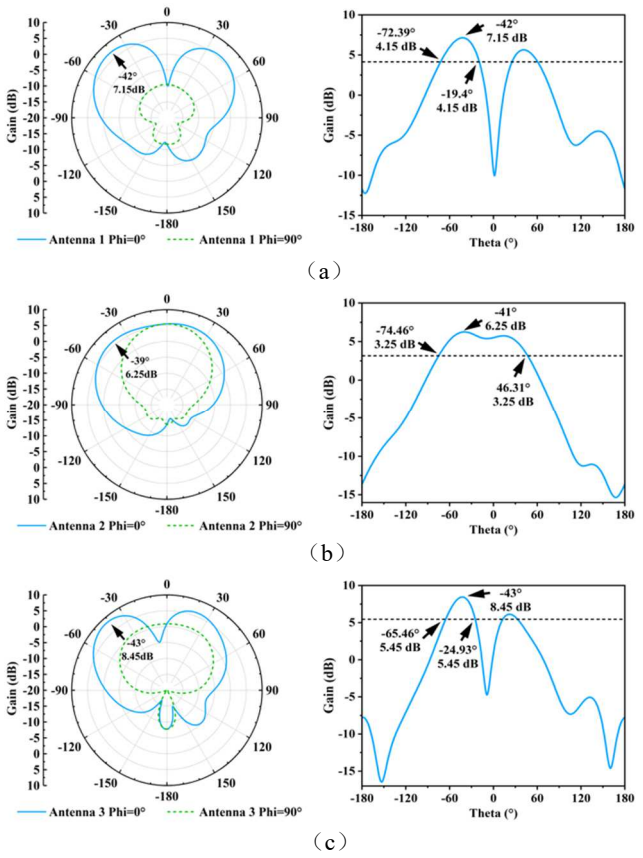

Fig. 6. Polar versus Cartesian direction diagrams obtained for the three antenna patterns (a) Antenna 1; (b) Antenna 2; (c) Antenna 3.

Array elements A1-A3, A6, A11-A14, A16, and A21-A23 are thermally activated to form Antenna 2's conductive configuration (Fig. 3(a)). This state implements a "W"-shaped radiating topology, reducing the effective electrical length and shifting the resonance frequency to 6.54 GHz (Fig. 5). The radiation pattern in Fig. 6(b) exhibits a maximum gain of 6.25 dB at elevation angle θ = -39° in the *xOz* plane, with a main lobe beamwidth of 120.77° spanning -74.46° to 46.31°.

Thermally activating array elements A1, A6-A7, A11-A13, A16-A17, and A21 establishes Antenna 3's conductive state (Fig. 4(a)). This triangular topology further reduces the effective electrical length, elevating the resonant frequency to 8.89 GHz (Fig. 5). The radiation pattern in Fig. 6(c) achieves a maximum gain of 8.45 dB at elevation angle θ = -43° in the *xOz* plane, with a 40.53° main lobe beamwidth spanning -65.46° to -24.93°.

Table II compares the electrical and radiation performance of Antennas 1-3. The beam pointing deviation remains within 4° across all states, indicating consistent radiation directionality. Gain variation is constrained to 2.2 dB while maintaining favorable radiation efficiency. Operating frequencies exhibit significant dispersion: 5.56 GHz, 6.54 GHz, and 8.89 GHz cover discrete C-X band segments with minimal spectral overlap, satisfying essential frequency reconfigurability requirements.

TABLE II. COMPARISON OF ANTENNA 1~3 KEY PARAMETERS

Results/ Configuration	**Antenna 1**	**Antenna 2**	**Antenna 3**
Operating Band (GHz)	5.48~5.62	6.52~6.56	8.77~8.99
Resonant Frequency (GHz)	5.56	6.54	8.89
Beam Direction (degrees)	-42	-39	-43
Beamwidth (degrees)	52.99	120.77	40.53
Gain (dBi)	7.15	6.25	8.45

IV. CONCLUSION

This paper proposes a frequency-reconfigurable pixelated antenna utilizing thermally controlled VO_2 phase-transition films. By dynamically mapping distinct radiating surfaces through VO_2's insulator-to-metal transition, three operational modes covering discrete C-X band segments are established. The antenna features a fabrication-friendly layout, with radiation efficiency critically dependent on VO_2 film quality-specifically, the conductivity contrast between insulating and metallic phases. Higher conductivity differentials yield superior electromagnetic radiation performance. Compared to electronic tuning approaches (e.g., RF-MEMS switches), this design eliminates bias circuitry, significantly reducing implementation complexity while positioning itself as a high-potential solution for adaptive wireless communication system.

REFERENCES

[1] H. Ö. Yılmaz and F. Yaman, "Metamaterial antenna designs for a 5.8-GHz Doppler radar," IEEE Trans. Instrum. Meas., vol. 69, no. 4, pp. 1775–1782, Apr. 2020.

[2] H. Zhang, T. Sun, W. Ren, C. Yuan, and D. Chen, "A novel dual-band printed monopole antenna with modified SIR loading," IEEE Access, vol. 12, pp. 13893–13899, 2024.

[3] B. K. Ahn, H.-W. Jo, J.-S. Yoo, J.-W. Yu, and H. L. Lee, "Pattern reconfigurable high gain spherical dielectric resonator antenna operating on higher order mode," IEEE Antennas Wireless Propag. Lett., vol. 18, no. 1, pp. 128–132, Jan. 2019.

[4] S. Arain, P. Vryonides, A. Quddious, and S. Nikolaou, "Reconfigurable BPF With Constant Center Frequency and Wide Tuning Range of Bandwidth," IEEE Trans. Circuits Syst. II Express Briefs, vol. 67, no. 8, pp. 1374–1378, Aug. 2020.

[5] Q. Xiang, Q. Feng, X. Huang, and D. Jia, "Electrical Tunable Microstrip LC Bandpass Filters With Constant Bandwidth," IEEE Trans. Microw. Theory Tech., vol. 61, no. 3, pp. 1124–1130, Mar. 2013.

[6] W. Kang, Y. Guo, L. Sang, T. Yuan, W. He, and W. Huang, "Function Reconfigurable RF Microstrip Filter Based on VO_2 Phase Transition," in 2023 International Conference on Microwave and Millimeter Wave Technology (ICMMT), Qingdao, China: IEEE, May 2023, pp. 1–3.

[7] E. Kusano, J. A. Theil, and J. A. Thornton, "Deposition of vanadium oxide films by direct-current magnetron reactive sputtering," J. Vac. Sci. Technol. Vac. Surf. Films, vol. 6, no. 3, pp. 1663–1667, May 1988.